JOURNAL OF MATERIALS SCIENCE: 27 (1992) 737–742

Model for the potential barrier depth along the grain boundaries of an ultrathin tin dioxide gas sensor

T. SUZUKI, T. NOMA, T. YAMAZAKI, N. IKEZAWA
Department of Applied Chemistry, Faculty of Technology, Tokyo University of Agriculture and Technology, Koganei, Tokyo 184, Japan

A potential barrier model along the grain boundaries in ultrathin tin dioxide (SnO_2) gas sensors is presented. It is assumed that the negatively charged oxygens are adsorbed only on the grain boundaries. The potential barrier depth is expressed as functions of grain size, donor concentration and surface coverage of adsorbed oxygen ions at the boundaries. A direct consequence is that the conduction electrons are effectively confined in a grain when the film thickness becomes smaller than a critical value. This indicates a drastic increase in resistivity with decreasing film thickness in air, and thus an occurrence of an extremely high gas sensitivity.

1. Introduction

It is generally accepted that the charged species such as O^- and O_2^- are adsorbed on the SnO_2 surface in air [1]. This trapping of conduction electrons and the resulting electrostatic potential induces an electron-depleted region, thus increasing resistivity parallel to the surface. In our previous studies of the thickness dependence of sensor properties in SnO_2 thin films [2, 3], a model was required which can interpret a drastic resistivity increase in air with decreasing thickness from about 100–10 nm. So far, most models proposed for semiconductor gas sensors assume the sites of ionosorbed oxygens to be distributed homogeneously on the whole surface of films or sintered porous bodies [4–6]. These models seem to produce potential barriers too small to interpret our experimental results. A model which assumes a distribution of ionosorbed oxygens only on the grain boundaries is proposed. The present model expresses the potential barrier depth along the grain boundaries as functions of grain size, donor concentration and surface coverage. An important result is that there exists a critical film thickness below which the conduction electrons are confined in a grain.

2. Theory

2.1. Potential at the surface

Yamazoe *et al.* [1] have shown that the surface coverage, θ_0, defined as the number of adsorbed O_2 molecules per surface tin atom, is less than 1%. Among the adsorbed oxygens, only those of negatively charged ions are our concern. Thus, for adsorbed O^- or O_2^-, we define θ instead of θ_0. If the mean distance of the surface tin atom is d_0 and that of charged oxygens is d, in the case when they are distributed uniformly on the whole surface, then, by definition

$$\theta = \frac{d_0^2}{d^2} \tag{1}$$

Because the lattice constant of the rutile structure is $a = 0.474$ nm and $c = 0.319$ nm [7], $d_0 = 0.4$ nm is a good approximation. Then we see, for example, that d becomes 4, 12.6 and 40 nm for $\theta = 1\%$, 0.1% and 0.01%, respectively. For the construction of grains, let us consider an array of parallel grain boundaries at the surface; the boundaries being infinitely long and with a uniform spacing, l, between them. Thus an array of square grains of length, l, is formed from these parallel boundaries as depicted schematically in Fig. 1. We also assume that the charged oxygens are all concentrated on these square boundaries. Therefore, the charge density, σ, of a grain boundary is

$$\sigma = -el/2d^2 = -e\theta l/2d_0^2 \tag{2}$$

where e is the charge of an electron.

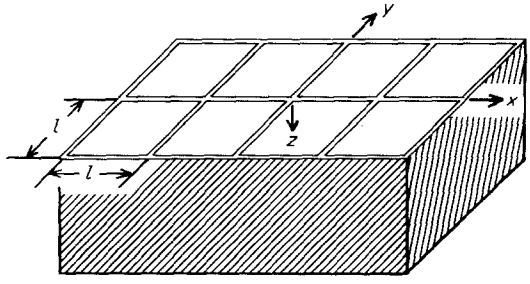

Figure 1 Surface grain structure. Two sets of parallel grain boundaries with a uniform spacing, l, between them form rectangular grains.

0022–2461/92 $03.00 + .12

Now we are ready to formulate the surface potential, ϕ_s. The potential from a single straight boundary lying on the y-axis is

$$\phi_s = -(\sigma/2\pi\varepsilon_0)\ln(x/x_0) \quad (3)$$

for $0 \leqslant x \leqslant x_0$. Here ε_0 is the dielectric constant in air and x_0 is a constant to be determined from the boundary condition. We choose $x_0 = l/2$ so that $\phi_s = 0$ at the middle of the two parallel boundaries. Then

$$\phi_s = -(\sigma/2\pi\varepsilon_0)\ln(2x/l) \quad (4)$$

for $x \leqslant l/2$. This corresponds to the nearest neighbour approximation; charges further than $l/2$ have no influence on the potential. This would be a good approximation, because an important potential is formed only near the boundary $1 \gg x/x_0$. Considering the periodic nature of the potential, it would be better to replace Equation 4 with

$$\phi_s = -(\sigma/2\pi\varepsilon_0)\ln(\sin\pi x/l) \quad (5)$$

This gives the potential curve as shown schematically in Fig. 2. For convenience, we expand the term $\ln(\sin\pi x/l)$ as the Fourier cosine series

$$\ln[\sin(\pi x/l)] = (a_0/2) + \sum_{m=1}^{\infty} a_m \cos(2\pi m x/l) \quad (6)$$

$$a_m = (4/l)\int_0^{l/2} \ln(\sin\pi x/l)\cos(2\pi m x/l)\,dx \quad (7)$$

where m is the harmonic number.

Integration of Equation 7 can be carried out with the help of the following formula:

$$\int_0^{\pi/2} \cos(2mx)\ln(\sin x)\,dx = -(\pi/4m) \quad (8)$$

and yields $a_m = -1/m$ and $a_0 = -1.386\,294$.

2.2. Bulk potential of one-dimensional boundaries

Let us assume that the donor concentration, N_d, is constant throughout the film and that all of them are singly ionized. For parallel boundaries along the y-axis, the bulk potential ϕ_b is uniform along the y-axis and it must satisfy the following Poisson's equation in the region where electrons are depleted

$$\nabla^2\phi_b(x, z) = -(eN_d/\varepsilon) \quad (9)$$

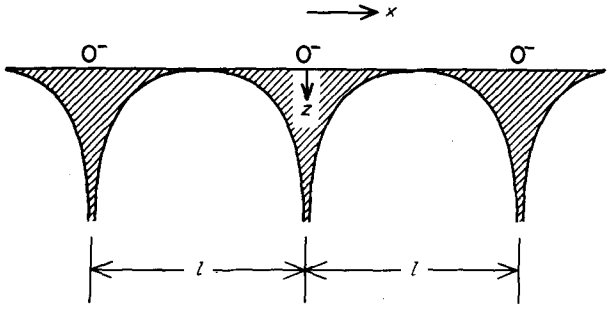

Figure 2 Surface potential of Equation 5. Charged grain boundaries extend parallel to the y-axis.

where ε is the dielectric constant of the film. The boundary condition is

$$\phi_b(x, 0) = \phi_s \quad (10)$$

To solve Equation 9, we make use of the principle of superposition and assume

$$\phi_b(x, z) = \phi_{b1}(x, z) + \phi_{b2}(z) \quad (11)$$

$$\nabla^2\phi_{b1}(x, z) = 0 \quad (12)$$

$$\nabla^2\phi_{b2}(z) = -(eN_d/\varepsilon) \quad (13)$$

It is natural to assume that ϕ_{b1} has the same periodicity with ϕ_s along the x-axis, thus we might try terms like

$$\phi_{b1}(x, z) = \sum_{m=0}^{\infty} \phi_{b1m}(x)F_m(z) \quad (14)$$

$$\phi_{b1m} = P_m\cos(2\pi m x/l) \quad (15)$$

Substituting Equations 14 and 15 into Equation 12, we obtain

$$d^2F_m(z)/dz^2 = (2\pi m/l)^2 F_m(z) \quad (16)$$

So we have

$$F_0(z) = B'z + C' \quad (17)$$

for $m = 0$, and

$$F_m(z) = Q_m\exp(-2\pi m z/l) \quad (18)$$

for $m \geqslant 1$.

Equation 13 gives

$$\phi_{b2}(z) = -(eN_d/2\varepsilon)z^2 + B''z + C'' \quad (19)$$

Thus, the solution of Equation 9 is expressed as the sum of ϕ_{b1} and ϕ_{b2} as

$$\phi_b(x, z) = \sum_{m=1}^{\infty} A_m\exp(-2\pi m z/l)\cos(2\pi m x/l) - (eN_d/2\varepsilon)z^2 + Bz + C \quad (20)$$

Equation 20 must satisfy the boundary condition of Equation 10, so putting $z = 0$, it becomes

$$\phi_b(x, 0) = \sum_{m=1}^{\infty} A_m\cos(2\pi m x/l) + C \quad (21)$$

Comparing this with Equations 5 and 6, we find the constants to be

$$A_m = -\frac{\sigma a_m}{2\pi\varepsilon_0} \quad (22)$$

and

$$C = -\frac{\sigma a_0}{4\pi\varepsilon_0} \quad (23)$$

Equation 20 then gives

$$\phi_b(x, z) = -(\sigma/2\pi\varepsilon_0)\sum_{m=1}^{\infty} a_m\exp(-2\pi m z/l)\cos(2\pi m x/l) - (eN_d/2\varepsilon)z^2 + Bz - (\sigma a_0/4\pi\varepsilon_0) \quad (24)$$

The constant B is determined from the simplified condition that the potential must smoothly vanish to zero at $x = 0$ and $z = z_0$. This condition would be enough to obtain the right value of the potential depth

just beneath a boundary. So we have

$$\phi_b(0, z_0) = 0 \quad (25)$$

and

$$\frac{d\phi_b(0, z_0)}{dz} = 0 \quad (26)$$

Trying Equation 26 in Equation 24, we have the constant

$$B = -(\sigma/\varepsilon_0 l)\sum_{m=1}^{\infty} a_m m \exp(-2\pi m z_0/l) + (eN_d z_0/\varepsilon) \quad (27)$$

Substituting this into Equation 24, we can solve Equation 25. We rewrite the solution referring to $a_m = -1/m$ and Equation 2. It gives

$$\sum_{m=1}^{\infty}[(1/m) + (2\pi z_0/l)]\exp(-2\pi m z_0/l) - (2\pi\varepsilon_0 d_0^2 N_d z_0^2/\varepsilon\theta l) - (a_0/2) = 0 \quad (28)$$

This gives z_0 and once z_0 is determined, the potential in the xz-plane can similarly be obtained by substituting Equation 27 into Equation 24.

The result is

$$-\left(\frac{4\pi\varepsilon_0 d_0^2}{e\theta l}\right)\phi_b(x, z) = \sum_{m=1}^{\infty}\left[\left(\frac{1}{m}\right)\cos\left(\frac{2\pi m x}{l}\right)\exp\left(-\frac{2\pi m z}{l}\right) + \left(\frac{2\pi z}{l}\right)\exp\left(-\frac{2\pi m z_0}{l}\right)\right] - \left(\frac{2\pi\varepsilon_0 d_0^2 N_d}{\varepsilon\theta l}\right)z(2z_0 - z) - \frac{a_0}{2} \quad (29)$$

Equation 29 is a fundamental one correlating the bulk potential to a depth of zero potential z_0 at the cross-point, grain size l, surface coverage θ and donor concentration N_d.

In the real sensor operation, temperture T is generally kept in the order of 100 K. Therefore, we then add the effect of thermal energy on the potential depth. The condition is that thermal energy E of an electron in one dimensional motion becomes equal to the potential energy at the depth z. Then

$$E = \frac{kT}{2} = -e\phi_b(x, z) \quad (30)$$

Inserting Equation 30 into Equation 29, we get

$$\sum_{m=1}^{\infty}[(1/m)\cos(2\pi m x/l)\exp(-2\pi m z/l) + (2\pi z/l)\exp(-2\pi m z_0/l)] - (2\pi\varepsilon_0 d_0^2 N_d/\varepsilon\theta l)z(2z_0 - z) - (a_0/2) - (2\pi\varepsilon_0 d_0^2 kT/e^2\theta l) = 0 \quad (31)$$

where $a_0 = -1.386294$.

3. Analysis of the theory

3.1. One-dimensional boundaries

We are now ready to practice the numerical calculation. Let us begin with the depth of zero potential, z_0, using Equation 28 with the constants $\varepsilon_0 = 8.854\,19 \times 10^{-12}\,\mathrm{F\,m^{-1}}$, $\varepsilon = 13.5\varepsilon_0$ [8], $k = 1.380\,66 \times 10^{-23}\,\mathrm{J\,K^{-1}}$ and $d_0 = 0.4$ nm. Summing m up to 500, we can obtain the potential depth z in the xz-plane according to Equation 31; z corresponds to the barrier depth against electrical conduction at elevated temperatures. For a grain boundary of $l = 1000$ nm with $\theta = 0.08\%$, the barrier depth is plotted in Fig. 3 as functions of distance and donor concentration for 573 K. The values obtained are acceptable. It indicates that important potential spreads only within the region very close to boundaries. For application to square grains, it is necessary to consider the conduction along a direction which crosses the boundaries as illustrated in Fig. 4. When a film thickness is larger than the barrier depth just beneath a boundary ($x = 0$), which we denote by $z = z_c$, the conduction electron can move freely at the bottom

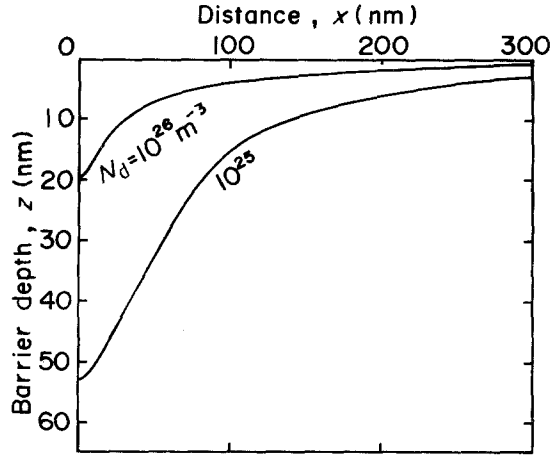

Figure 3 Barrier depth at 300 °C as functions of distance and donor concentration for $l = 1000$ nm and $\theta = 0.08\%$.

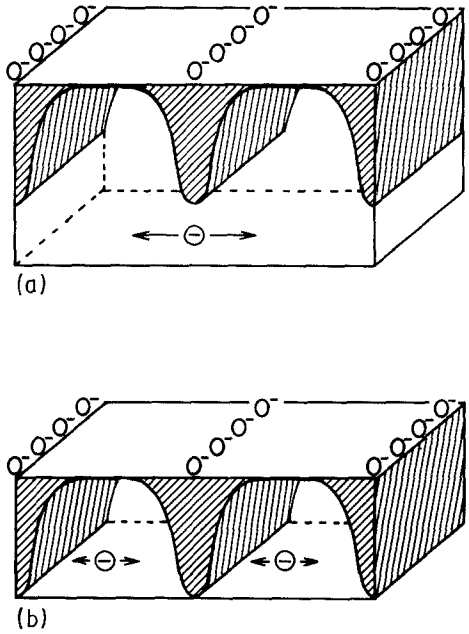

Figure 4 Schematic representation of barrier depth, film thickness and motion of electrons in a direction which crosses boundaries. (a) When films are thicker than barrier depth, electrons can move freely at the bottom part. (b) Electrons are confined in a grain in films thinner than barrier depth.

part of the film (Fig. 4a). On the other hand, electrons are confined in a grain in films thinner than z_c. Thus we see that the potential barrier depth, z_c, corresponds to critical film thickness below which conduction cannot occur. Then we need to examine the effect of temperature on this barrier depth.

The thermal term in Equation 31 is expressed, using the number of electrons per unit boundary length, n,

$$n = l\theta/2d_0^2 \tag{32}$$

as $2\pi\varepsilon_0 d_0^2 kT/e^2\theta l = \pi\varepsilon_0 kT/ne^2$. If we limit the range of n from 0.25–25 electrons per nm, the thermal term gives the largest value of 0.034 29 when $n = 0.25$ for $T = 573$ K. The value is very small compared with $-a_0/2 = 0.693\,15$. In fact, temperature dependence of barrier depth z_c is small even at elevated temperature of 800 K as shown in Fig. 5 for $l = 1000$ nm and $\theta = 0.08\%$. So, the following discussion assumes a constant temperature of 573 K. Fig. 6 shows the barrier depth as functions of grain size and donor concentration at a given surface coverage of $\theta = 0.008\%$, 0.08% and 0.8%, respectively. In the figure, upper and lower limits of curves correspond to $n = 0.25$ and 25

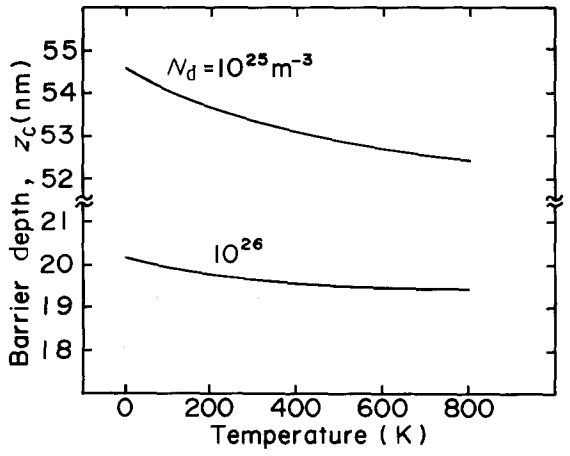

Figure 5 Temperature dependence of barrier depth for $l = 1000$ nm and $\theta = 0.08\%$.

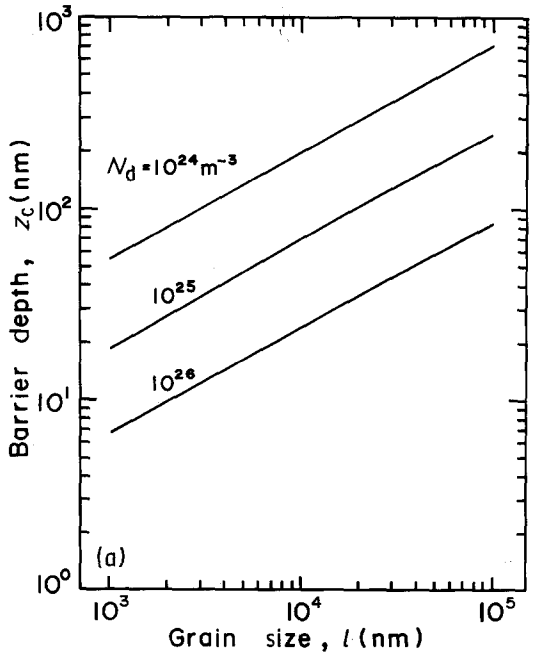

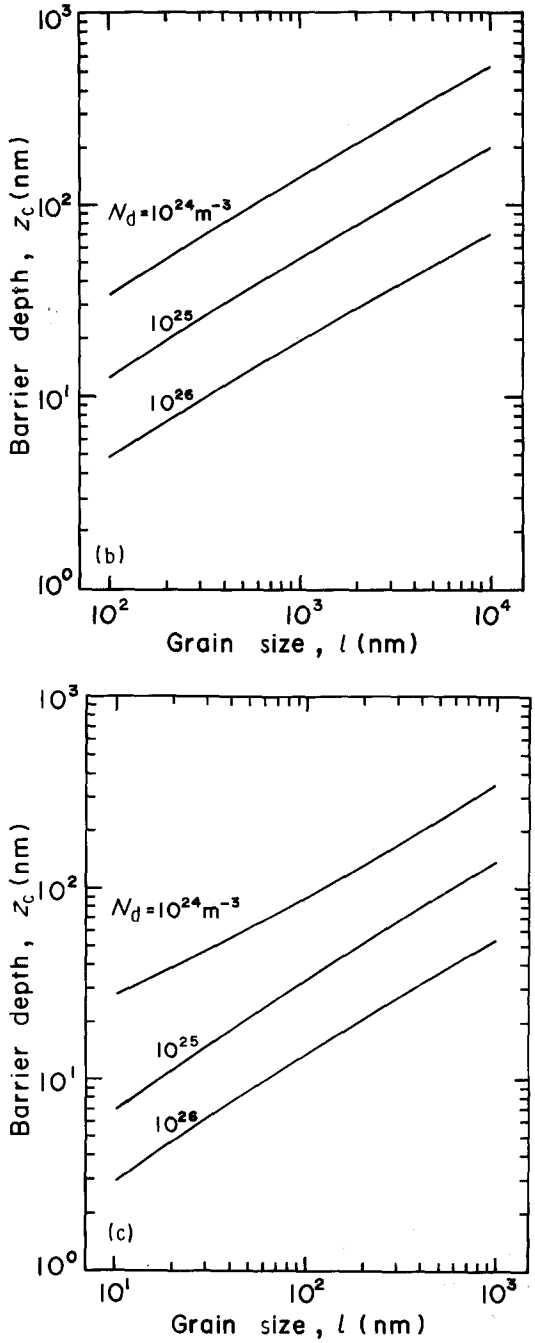

Figure 6 Barrier depth as functions of grain size and donor concentration at 300 °C. (a) $\theta = 0.008\%$, (b) $\theta = 0.08\%$, (c) $\theta = 0.8\%$.

electrons/nm. The upper limit may seem a little denser than expected from the line boundary model. However, real boundaries are more complicated than a mere line, and so we prefer including such a denser situation. It is evident that the barrier depth increases rapidly with increasing grain size and decreasing donor concentration. Fig. 7 gives the barrier depth as functions of donor concentration and surface coverage for $l = 1000$ nm. It is noted that a lower donor concentration gives a steeper increase in barrier depth with increased surface coverage compared with a higher donor concentration.

3.2 Rectangular grains

The principle of superposition tells us that the bulk potential in rectangular grains, $\phi_b(x, y, z)$, can be expressed as the sum of potential from one-dimensional

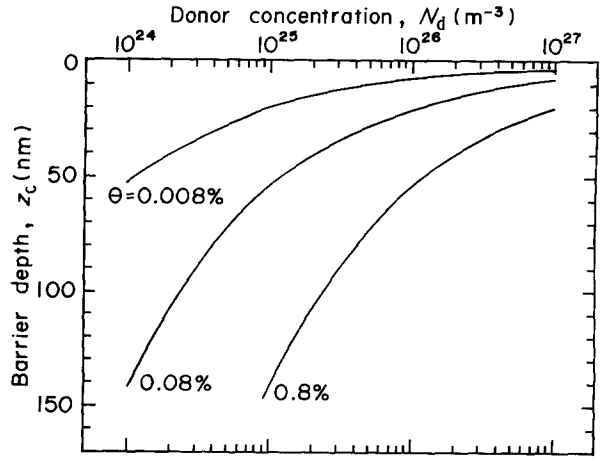

Figure 7 Barrier depth as functions of donor concentration and surface coverage at 300 °C for $l = 1000$ nm.

grain boundaries crossing at right angles

$$\phi_b(x, y, z) = \phi_b(x, z) + \phi_b(y, z) \qquad (33)$$

Thus numerical solution of the potential barrier depth is readily obtained from our previous results. The potential barrier curve surrounding a grain is illustrated schematically in Fig. 8. Thus we come across the same conclusion as in Section 3.1, that z_c corresponds to the critical film thickness for electrical conduction in any direction parallel to the surface. Having understood the importance of the barrier depth, z_c, let us now try to explain our experimental results in ultrathin SnO_2 gas sensors obtained against 0.5% H_2 at 300 °C. However, the discussion is only qualitative, because we do not have exact values of grain size, donor concentration and surface coverage. So far, experiments showed two prominent features in ultrathin sensors in air. One is a highly constant resistivity in films thinner than about 10 nm [3] and the other is a steeply increasing resistivity with annealing time [2] as depicted schematically in Fig. 9. The former indicates that the barrier depth, z_c, is about 10 nm. For the latter, we observed a resistivity increase of more than four orders of magnitude when about 17 nm thick films were annealed for 100 h at 500 °C in air. The slope became steeper with prolonged annealing time. This enormous change can be interpreted as a result of increased barrier depth. Suppose a film is several times

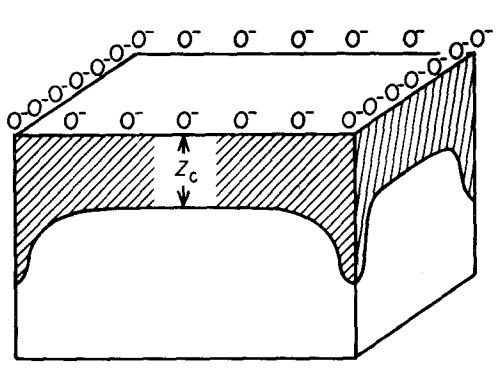

Figure 8 Schematic illustration of barrier depth variation under grain boundaries in a rectangular grain.

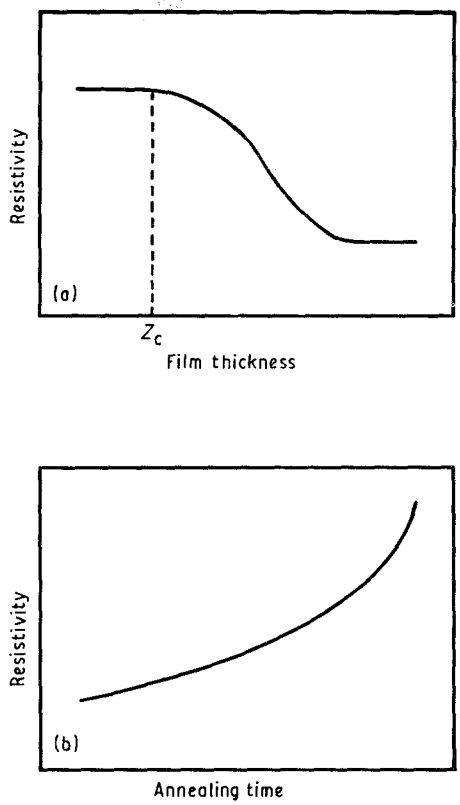

Figure 9 Schematic representation of resistivity behaviour in ultrathin SnO_2 films in air at 300 °C. (a) Resistivity increases steepy with decreasing film thickness and remains at a high value when films become thinner than about 10 nm [3]. (b) Resistivity increases more and more sharply with prolonged annealing time at 500 °C in 15–18 nm thick films [2].

thicker than z_c at the beginning of annealing. Resistivity will increase with increasing z_c up to a depth a little smaller than about 17 nm. Further increase in z_c will cause a steeper increase in resistivity, as experiment revealed. Increase in z_c is a result of grain growth, donor annihilation or increased surface coverage after annealing, as Figs 6 and 7 predict. It is not certain whether or not the surface coverage increases by annealing. For further discussions, we need observation of grain boundaries and detailed electrical measurements to determine the donor concentration and mobility in ultrathin films.

4. Conclusion

A potential barrier model is proposed for ultrathin SnO_2 gas sensors. The model assumes rectangular grain boundaries on which all ionosorbed oxygens concentrate. Potential in the film is expressed as functions of grain size, donor concentration and surface coverage. The model yields an acceptable value of potential barrier depth which corresponds to critical film thickness. Below the critical thickness, electrical conduction parallel to the surface becomes impossible and electrons are confined in a grain. The potential barrier depth becomes larger with grain growth, donor annihilation and increased surface coverage. The model predicts a high resistivity for films thinner

than a critical value and a larger rate of increasing resistivity with prolonged annealing time for films several times thicker than the critical thickness initially.

References

1. N. YAMAZOE, J. FUCHIGAMI, M. KISHIKAWA and T. SEIYAMA, *Surface Sci.* **86** (1979) 335.
2. T. SUZUKI and T. YAMAZAKI, *J. Mater. Sci. Lett.* **9** (1990) 750.
3. T. SUZUKI, T. YAMAZAKI, K. HAYASHI and T. NOMA, *J. Mater. Sci.* (to be published).
4. S. SAKAI, M. NAKAGAWA, I. DOI and M. MITSUDO, Denkiagakkai Denshisouchi Kenkyuukai Shiryou EDD-75-50 (1975).
5. H. WINDISCHMANN and P. MARK, *J. Electrochem. Soc.* **126** (1979) 627.
6. P. ROMPAINEN and V. LANTTO, *J. Appl. Phys.* **63** (1988) 5159.
7. JCPDS 21–1250, (1953).
8. R. SUMMITT, *J. Appl. Phys.* **39** (1968) 3768.

Received 8 October 1990
and accepted 20 March 1991